Scintillations of higher-order optical beams in biological tissues

Baykal, Yahya; Gökçe, Muhsin Caner; Ata, Yalçın; Gerçekcioğlu, Hamza

DOI
10.1364/JOSAB.555713

Publication date
2025

Document Version
Final published version

Published in
Journal of the Optical Society of America B: Optical Physics

Journal of the Optical Society of America B
OPTICAL PHYSICS

Scintillations of higher-order optical beams in biological tissues

Yahya Baykal,[1,*] Muhsin Caner Gökçe,[2,3] Yalçın Ata,[4] and Hamza Gerçekcioğlu[5]

[1]Çankaya University, Department of Electrical and Electronics Engineering, Yukarıyurtçu mah. Mimar Sinan Cad. No: 4, Etimesgut 06815, Ankara, Turkey
[2]TED University, Department of Electrical and Electronics Engineering, Ziya Gökalp cad. No: 47-48, Kolej, 06420 Çankaya, Ankara, Turkey
[3]Delft University of Technology, Department of Geoscience and Remote Sensing, Delft, The Netherlands
[4]OSTİM Technical University, Department of Electrical and Electronics Engineering, 100. Yıl Bulvarı OSTİM, 06374 Yenimahalle, Ankara, Turkey
[5]Republic of Turkish Ministry of Transport and Infrastructure, Ankara, Turkey
*y.baykal@cankaya.edu.tr

Received 13 January 2025; revised 17 February 2025; accepted 3 March 2025; posted 3 March 2025; published 27 March 2025

The Scintillation index of a higher-order laser beam in turbulent biological tissue is formulated and evaluated. Behaviors of the scintillation indices of various higher-order beams against the tissue turbulence parameters of the strength coefficient of the refractive index fluctuations, fractal dimension, characteristic length of heterogeneity, small length-scale factor, and the source size, tissue length, and wavelength are examined. Fluctuations in the intensity are also investigated when various types of tissues, such as the intestinal epithelium (mouse), liver parenchyma (mouse), and upper dermis (human), are excited by different higher-order laser beams.

https://doi.org/10.1364/JOSAB.555713

1. INTRODUCTION

The interaction of optical waves with biological tissues is becoming important in diagnostics and treatment issues. Propagation properties of different optical beams in a turbulent tissue medium are studied [1–9]. In these works, in a turbulent tissue, beam spreading and wander of partially coherent Lommel–Gaussian beams [1], propagation properties of anomalous hollow beams [2], coherent Laguerre–Gaussian beams [3], laser array propagation through liver [4], characteristics of partially coherent circular flattened Gaussian vortex beams [5], annular beam in liver [6], propagation of stochastic electromagnetic vortex beams [7], statistical properties of anisotropic electromagnetic [8], and propagation properties of hollow Gaussian beams [9] are reported.

Intensity fluctuations quantified by the scintillation index are evaluated in different turbulent media for many different types of optical sources. We have recently explored the field correlation characteristics of multimode beams in tissue turbulence [10], from which field correlations of higher-order optical beams in tissue turbulence can be obtained.

In turbulent tissue, scintillations of optical waves are evaluated in weak [11,12] and in any strength of turbulence [13]. Finally, we have summarized the tissue turbulence in general and its effects on optical waves in a recent review paper [14].

In this paper, we formulated and evaluated the scintillation index in turbulent tissue when higher-order optical excitations are used. Variations of the scintillation against the source, tissue, and turbulence parameters are exhibited. Our results are also applied to some specific tissue types. Findings in this paper will be of use to researchers who study tissue engineering in diagnostics, imaging, and treatment applications.

2. FORMULATION

A higher-order mode source field is given by [15]

$$u(\mathbf{s}) = H_n(s_x/\alpha_s)\, H_m(s_y/\alpha_s) \exp\left[-0.5\alpha_s^{-2}(s_x^2 + s_y^2)\right] \quad (1)$$

where $\mathbf{s} = (s_x, s_y)$ is the transverse source coordinate, $H_n(\cdot)$ and $H_m(\cdot)$ are the Hermite polynomials, n and m being the mode numbers of the higher-order mode laser beams in x and y directions, and α_s is the Gaussian source size denoting the radius.

Previously, we have obtained the log-amplitude correlation function B_χ for a general-type beam propagating in turbulence [16]. A special case of the general beam is the higher-order mode. It is known that in weak turbulence, the scintillation index is given by $m^2 = 4B_\chi$ [17], where B_χ is the correlation function of the log amplitude of the random field fluctuations at the origin of the observation plane, originating from the tissue turbulence, and m^2 denotes the scintillation index occurring as the result of randomly fluctuating fields in the tissue due to tissue turbulence.

To find the field at the receiver point $\mathbf{r} = (\mathbf{p}, z) = (p_x, p_y, z)$ in the absence of turbulence, the Huygens–Fresnel principle is employed. By defining this field as the free-space field, $u^{FS}(\mathbf{p}, z)$, and using the source field for the higher-order mode beam given in Eq. (1), $u^{FS}(\mathbf{p}, z)$ is found to be

$$u^{FS}(\mathbf{p}, z) = \frac{k \exp(ikz)}{2\pi i z} \int_{-\infty}^{\infty}\int_{-\infty}^{\infty} \mathbf{d^2 s} H_n(s_x/\alpha_s)\, H_m(s_y/\alpha_s) \times \exp\left[-0.5\alpha_s^{-2}(s_x^2 + s_y^2)\right] \exp\left[\frac{ik}{2z}(\mathbf{s} - \mathbf{p})^2\right], \tag{2}$$

where $k = 2\pi/\lambda$ is the wavenumber, and λ is the beam wavelength. By performing the integration over $\mathbf{s} = (s_x, s_y)$ through the help of Eq. (7.374.8) of Ref. [18], and after rearrangements, $u^{FS}(\mathbf{p}, z)$ is obtained as

$$u^{FS}(\mathbf{p}, z) = \frac{k}{\gamma^*} e^{ikz}\left(\frac{\gamma}{\gamma^*}\right)^{(n+m)/2} \exp\left[-\frac{0.5k\alpha_s^{-2}}{\gamma^*}\left(p_x^2 + p_y^2\right)\right] \times H_n\left\{[k^2\alpha_s^{-1}(\gamma^*\gamma)^{-1/2}]p_x\right\} H_m\left\{[k^2\alpha_s^{-1}(\gamma^*\gamma)^{-1/2}]p_y\right\}, \tag{3}$$

where $\gamma = k - i\alpha_s^{-2}z$, $i = (-1)^{0.5}$, and * denotes the complex conjugate. By employing the free-space field, $u^{FS}(\mathbf{p}, z)$ in Eq. (3), the field at the receiver plane in the presence of turbulence is given by the Rytov method as [16]

$$u(\mathbf{p}, z) = u^{FS}(\mathbf{p}, z) \exp\left[\psi(\mathbf{p}, z)\right], \tag{4}$$

where

$$\psi(\mathbf{p}, z) = \chi(\mathbf{p}, z) + iS(\mathbf{p}, z) = \frac{k^2}{2\pi u^{FS}(\mathbf{p}, z)} \int_{V'} \mathrm{d}^3 r' n_1(\mathbf{p}', z')\, u^{FS}(\mathbf{p}', z') \times \frac{\exp\left(ik|\mathbf{r} - \mathbf{r}'|\right)}{|\mathbf{r} - \mathbf{r}'|} \tag{5}$$

is the complex amplitude fluctuation in turbulence, $\chi(\mathbf{p}, z)$ and $S(\mathbf{p}, z)$ are the log-amplitude and phase fluctuations, respectively, and $u^{FS}(\mathbf{p}', z')$ is the field in free space (i.e., in the absence of turbulence) at $\mathbf{r}' = (\mathbf{p}', z') = (p_x', p_y', z')$. Note that the integration in Eq. (5) is taken over the volume V', i.e., $d^3r' = dp_x'dp_y'dz'$, and n_1 is the random part of the refractive index, which is [16]

$$n_1(p_x', p_y', z') = \int_{-\infty}^{\infty}\int_{-\infty}^{\infty} \exp\left(i\kappa_x p_x' + i\kappa_y p_y'\right) \mathrm{d}Z_n(\kappa_x, \kappa_y, z'), \tag{6}$$

where κ_x and κ_y are the spatial frequencies in x and y directions, $dZ_n(\kappa_x, \kappa_y, z')$ is the random amplitude of the spectrum of the refractive index fluctuations where the integrations are implicit with respect to κ_x and κ_y. By applying the paraxial approximation to Green's function term $\frac{\exp(ik|\mathbf{r}-\mathbf{r}'|)}{|\mathbf{r}-\mathbf{r}'|}$ in Eq. (5), substituting Eqs. (3) and (6) into Eq. (5), and performing the $dp_x'dp_y'$ integrations through the use of Eq. (7.374.8) in [18], the fluctuations of the complex amplitude in turbulence at the receiver plane are found at $z = L$, where L is the tissue length. Thus, the found $\psi(\mathbf{p}, z)$ is for higher-order optical beams. The remaining part of the derivation follows the similar steps as in Appendix A of Ref. [19] [starting from Eq. (A5)], where the free-space field, $u^{FS}(\mathbf{p}, z)$, given by Eq. (3) of the current paper, is used instead of the free-space field, $u_{n,m}^{FS}(\mathbf{p}, z)$ used in Ref. [19]. We prefer not to repeat the lengthy derivation in the current paper, but utilizing the formulation in Appendix A of Ref. [19], the log-amplitude correlation function for the higher-order beam in turbulence is presented which reads as

$$B_\chi = \frac{\pi}{[H_n(0)\, H_m(0)]^2}\mathrm{Re} \times \left\{\int_0^L \mathrm{d}\eta \int_0^\infty \kappa\,\mathrm{d}\kappa \int_0^{2\pi} \mathrm{d}\varphi[V(\eta, \kappa, \varphi)\, V(\eta, -\kappa, \varphi) + |V(\eta, \kappa, \varphi)|^2]\Phi_n(\kappa)\right\}. \tag{7}$$

Thus, the scintillation index of the higher-order beam in tissue turbulence is written as $m^2 = 4B_\chi$. Here, η is the distance parameter along the propagation axis, Re denotes the real part, $|\cdot|$ represents the absolute value,

$$V(\eta, \kappa, \varphi) = ik \exp\left[-0.5i(k\beta)^{-1}(L - \eta)(k\alpha_s^2 + i\eta)\kappa^2\right] \times H_n[(\beta^*)^{-1}\alpha_s(\eta - L)\kappa\cos\varphi] \times H_m[(\beta^*)^{-1}\alpha_s(\eta - L)\kappa\sin\varphi], \tag{8}$$

where $\beta = k\alpha_s^2 + iL$, and $\Phi_n(\kappa)$ is power spectrum of tissue turbulence expressed as [20,21]

$$\Phi_n(\kappa) = \frac{Sl_c^3\Gamma(D_f/2)}{\pi^{3/2}2^{(5-D_f)/2}(1 + \kappa^2 l_c^2)^{D_f/2}} \exp\left(\frac{-\kappa^2\eta_0^2}{8\ln 2}\right), \tag{9}$$

where S is the strength coefficient of the refractive index fluctuations, D_f is the fractal dimension, l_c is the characteristic length of heterogeneity, η_0 is the small length-scale factor, and $\Gamma(\cdot)$ is the gamma function.

3. RESULTS

In this paper, the results are obtained through theoretical analysis and MATLAB simulations. The figures in this section are drawn by numerically evaluating B_χ, which is provided in Eq. (7) in order to obtain the scintillation index $m^2 = 4B_\chi$.

All the mode numbers, n, m, and the other necessary parameter values, are given in the legends and the horizontal axes of the figures. If not indicated in the legends of the figures, parameter values used are $S = 10^{-4}$, $D_f = 2.67$, $l_c = 10.24$ μm, $\eta_0 = 1$ μm, $\lambda = 0.633$ μm, $L = 3$ cm [except in Fig. 2(b), $L = 5$ cm], and $\alpha_s = \sqrt{\lambda L}$. In Fig. 8, scintillations of higher-order beams in some specific tissue types are

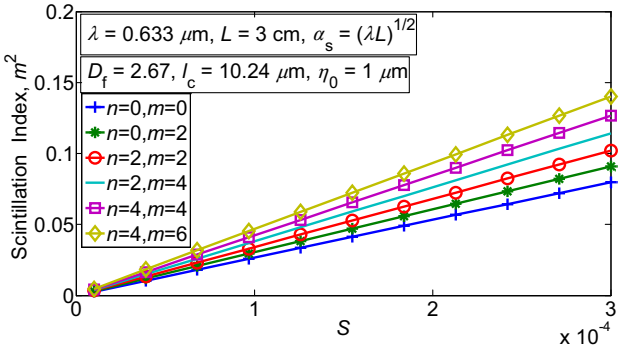

Fig. 1. Scintillation index in tissues versus S for different higher-order modes.

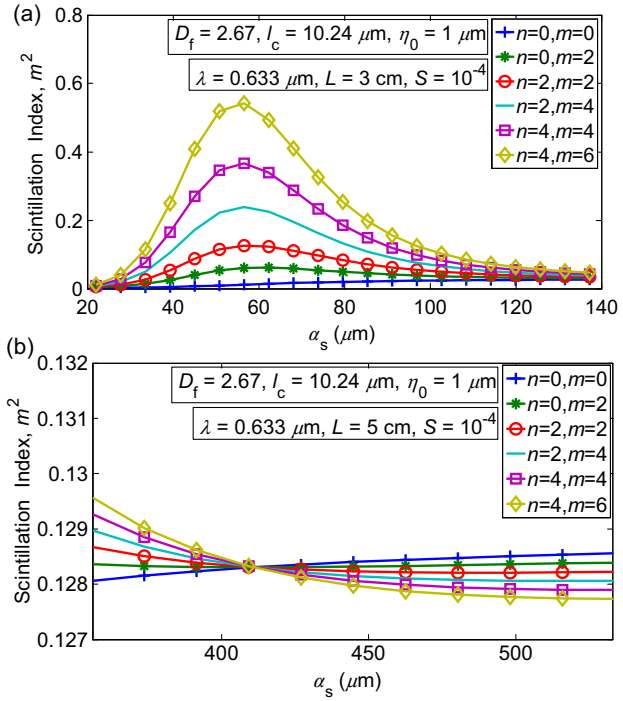

Fig. 2. (a) Scintillation index in tissues versus α_s for different higher-order modes. (b) Scintillation index in tissues versus α_s for different higher-order modes at larger L and larger α_s.

also examined. These tissue types are intestinal epithelium (mouse), liver parenchyma (mouse), and upper dermis (human) with turbulence parameters of $D_f = 2.67$, $l_c = 11.48$ μm; $D_f = 2.60$, $l_c = 10.24$ μm; and $D_f = 2.67$, $l_c = 5.24$ μm, respectively [22].

Three types of tissue that are the intestinal epithelium (mouse), liver parenchyma (mouse), and upper dermis (human) are employed in Fig. 8 only. In the remaining figures, general tissues (not specific types) with the mentioned realistic turbulence parameters are investigated. That is why in the captions of the remaining figures, just "tissues" are stated. In Fig. 1, being valid for all the higher-order modes, the scintillation index increases as the strength coefficient of the refractive index fluctuations increases. At a fixed value of the strength coefficient of the refractive index fluctuations, Fig. 1 shows that the scintillations become larger for high orders. However, this trend depends on the source and tissue parameters. To clarify this, Figs. 2(a) and 2(b) are provided. Figure 2(a) is drawn versus relatively smaller source sizes at the tissue length of 3 cm, and it is shown from Fig. 2(a) that the trend in Fig. 1 is valid, i.e., larger mode numbered higher-order modes attain larger scintillations. In Fig. 2(a), the trend of the scintillations of higher-order modes against the source size is that the scintillations increase at the relatively smaller source sizes. When the source size is further increased, the scintillations tend to decrease. This trend is due to the intensity profiles of the higher-order modes. In the case of the Gaussian beam ($n = m = 0$) in Fig. 2(a), the trend of the scintillations along the whole range of the source sizes is a continuous increase, which checks the classical result that in weak turbulence, scintillations continuously increase from spherical to plane wave. However, in Fig. 2(b), which is drawn at larger source sizes and at the tissue length of 5 cm, a transition of the trend is observed. At relatively smaller source sizes, the trend is the same as in Figs. 1 and 2(a), i.e., larger scintillations occur at higher-order modes with larger mode numbers. Figure 2(b) reflects that as the source size becomes larger, the trend reverses and this time smaller scintillations occur at higher-order modes with larger mode numbers. The reason to choose $L = 3$ cm in Fig. 2(a) is to keep the scintillations in the weak turbulence regime. When L in Fig 2(a) is chosen to be 5 cm, then the scintillations well exceed the unity, which does not fall in the weak tissue turbulence. The reason to choose $L = 5$ cm in Fig. 2(b) is that the transition of the trend in the scintillations is much more evident as compared to the case when L is chosen as 3 cm. Additionally, for the source sizes in Fig. 2(b), the scintillation values still remain in the weak tissue turbulence regime. Figure 3 indicates that the scintillations of all the higher-order modes increase when the fractal dimension increases. For the parameters chosen in Fig. 3, it is observed that modes with higher-order numbers have larger scintillations. Parameters chosen in Fig. 3 and in the other figures in this section (except in Fig. 8) are for general tissue types, i.e., not for a specific tissue, with the mentioned realistic turbulence parameters. Figure 4 shows that in the tissues having longer tissue length, any higher-order beam will have a larger scintillation index.

As shown in Fig. 5, scintillations of all higher-order optical beams increase as the characteristic length of heterogeneity increases. For the chosen source, tissue, and turbulence parameters, at the same characteristic length of heterogeneity, higher-order modes with larger mode numbers exhibit larger intensity fluctuations. When other parameters are kept fixed,

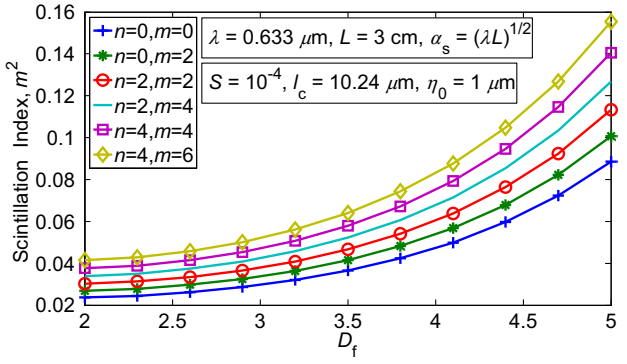

Fig. 3. Scintillation index in tissues versus D_f for different higher-order modes.

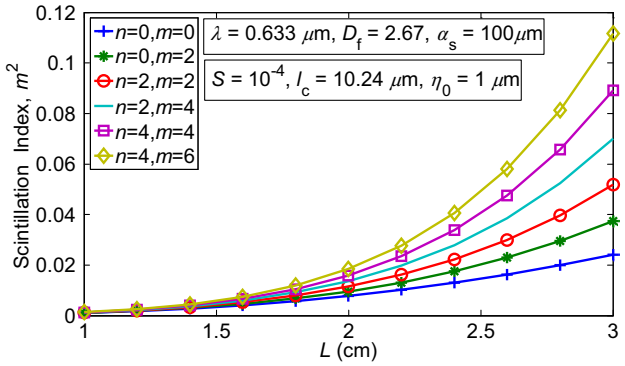

Fig. 4. Scintillation index in tissues versus L for different higher-order modes.

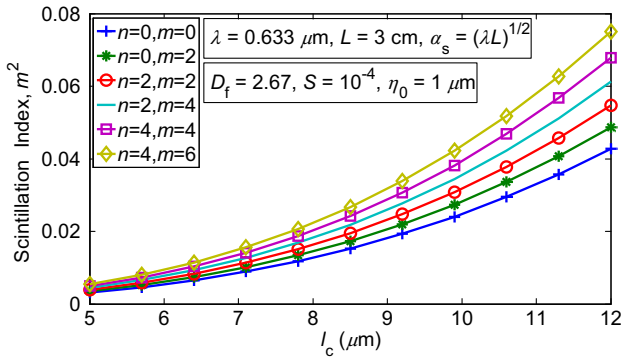

Fig. 5. Scintillation index in tissues versus l_c for different higher-order modes.

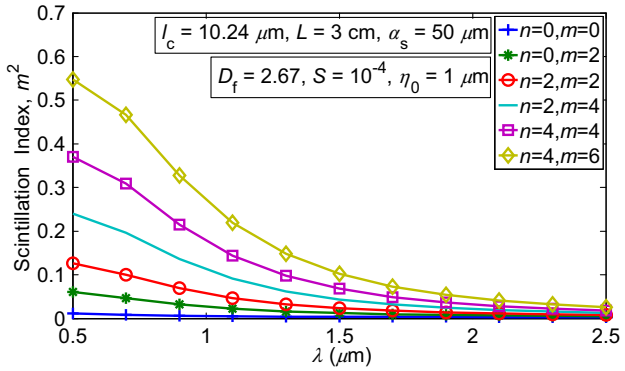

Fig. 6. Scintillation index in tissues versus λ for different higher-order modes.

Fig. 6 reveals that an increase in the wavelength, i.e., a decrease in the operating frequency, reduces the scintillations, and this trend is valid for all the higher-order modes. Again, by keeping the other parameters fixed, an increase in the small length-scale factor will reduce the scintillation index of all the higher-order modes, as shown in Fig. 7.

In Fig. 8, three different types of tissues are chosen that are intestinal epithelium (mouse), liver parenchyma (mouse), and upper dermis (human), and they are excited by various higher-order modes. Under these conditions, the scintillations in such tissues are evaluated. It is observed in Fig. 8 that an increase in the strength coefficient of the refractive index fluctuations

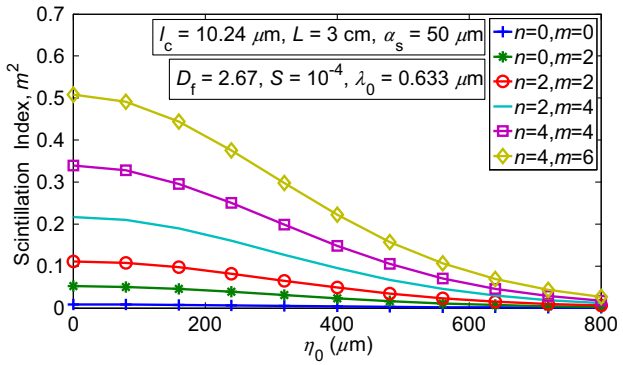

Fig. 7. Scintillation index in tissues versus η_0 for different higher-order modes.

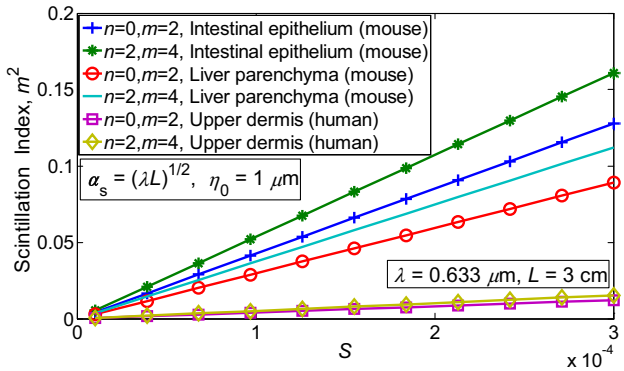

Fig. 8. Scintillation index in tissues versus S for different higher-order modes and different tissue types.

causes the scintillations of all higher-order modes to increase. At the same strength coefficient of the refractive index fluctuations and for the same higher-order mode, the intensity fluctuates the most in the intestinal epithelium (mouse) tissue and the least in the upper dermis (human) tissue.

From the plots in Figs. 1 and 3–7, the expected conclusion is that stronger tissue turbulence, i.e., a larger strength coefficient of the refractive index fluctuations, fractal dimension, tissue length, characteristic length of heterogeneity and smaller wavelength, and small length-scale factor, results in larger scintillations of any higher-order mode.

As apparent from Figs. 1, 2(a), and 3–8 and as explained in the explanations of some of these figures, as the mode number increases, the scintillation index becomes larger. However, as also mentioned in the explanation for Fig. 1, this is not a general trend, but the variation depends on the chosen source and tissue parameters. The change in the trend is shown in Fig. 2(b). Similarly, the trend of the scintillations against the strength coefficient of the refractive index fluctuations, fractal dimension, tissue length, characteristic length of heterogeneity, wavelength, small length-scale factor, and the different types of tissues will differ if the source and tissue parameters in Figs. 1, 2(a), and 3–8 are chosen accordingly.

The results presented in this paper can be employed in biomedical research and tissue engineering, and they will have potential applications in determining the deterioration or disruption of biological tissue, medical diagnosis, and medical

imaging. For a specific healthy tissue, tissue turbulence parameters have known characteristic values. When such a healthy tissue is excited with a higher-order optical beam, using the methods developed in this paper, the scintillation index can easily be evaluated. However, in a malignant tissue, turbulence parameter values will differ from the healthy tissue turbulence parameter values, resulting in a different scintillation as compared to the scintillation in a healthy tissue. By evaluating the higher-order mode scintillation index in the healthy and malignant tissues, the difference in the scintillation index will expose information on the malignancy of the tissue, which can be used to find out any anomalies in the tissue. By the application of such evaluations, the results presented in this paper can be linked to improving the imaging techniques or medical interventions. It is noted that related to the results presented in this section, there are clinical implications and practical applications in medical imaging and biomedical research, and the references some of which are detailed and provided in Ref. [23]. Thus, our results in this paper will be helpful in diagnosing the malignancy in the tissue. By utilizing the numerous intensity profiles of the higher-order optical beam, the diagnosis in the tissue can easily be localized, which is an important advantage of the higher-order beams.

4. CONCLUSION

Scintillation index is formulated and evaluated when a turbulent biological tissue is excited by higher-order optical beams. As known, higher-order beams are optical profiles that compose a multimode beam. The effect of tissue turbulence on the scintillations shows similar behavior for all the higher-order modes, which manifests itself as an increase in the intensity fluctuations when the strength coefficient of the refractive index fluctuations, fractal dimension, characteristic length of heterogeneity, and tissue length increase, and/or wavelength and small length-scale factor decrease, i.e., when the tissue turbulence experiences stronger regime.

At the same strength of turbulence in the tissue, the comparison of the scintillation values for the higher-order beams of different mode numbers depends on what the tissue length and the optical source parameters are.

Results of our work in this paper can be employed in tissue engineering research in applications, such as biomedical diagnosis.

Disclosures. The authors declare no conflicts of interest.

Data availability. The data that support the findings of this study are available upon reasonable request from the authors.

REFERENCES

1. L. Yu and Y. Zhang, "Beam spreading and wander of partially coherent Lommel–Gaussian beam in turbulent biological tissue," J. Quant. Spectrosc. Ra. **217**, 315–320 (2018).
2. X. Lu, X. Zhu, K. Wang, *et al.*, "Effects of biological tissues on the propagation properties of anomalous hollow beams," Optik **127**, 1842–1847 (2016).
3. A. A. Ebrahim and A. Belafhal, "Effect of the turbulent biological tissues on the propagation properties of coherent Laguerre-Gaussian beams," Opt. Quant. Electron. **53**, 179 (2021).
4. M. C. Gökçe, Y. Baykal, and Y. Ata, "Laser array beam propagation through liver tissue," J. Visual. **23**, 331–338 (2020).
5. Y. Ni, Y. Zhou, G. Zhou, *et al.*, "Characteristics of partially coherent circular flattened Gaussian vortex beams in turbulent biological tissues," Appl. Sci.-Basel **9**, 969 (2019).
6. M. C. Gökçe and Y. Baykal, "Effects of liver tissue turbulence on propagation of annular beam," Optik **171**, 313–318 (2018).
7. M. Luo, Q. Chen, L. Hua, *et al.*, "Propagation of stochastic electromagnetic vortex beams through the turbulent biological tissues," Phys. Lett. A **378**, 308–314 (2014).
8. X. Liu and D. Zhao, "The statistical properties of anisotropic electromagnetic beams passing through the biological tissues," Opt. Commun. **285**, 4152–4156 (2012).
9. F. Saad and A. Belafhal, "A theoretical investigation on the propagation properties of hollow Gaussian beams passing through turbulent biological tissues," Optik **141**, 72–82 (2017).
10. Y. Baykal, M. C. Gökçe, H. Gerçekcioğlu, *et al.*, "Correlations of multimode optical incidences in turbulent biological tissue," J. Opt. Soc. Am. A **40**, 2045–2051 (2023).
11. Y. Baykal, Ç. Arpali, and S. A. Arpali, "Scintillation index of optical spherical wave propagating through biological tissue," J. Mod. Opt. **64**, 138–142 (2017).
12. H. Jin, W. Zheng, H. Ma, *et al.*, "Average intensity and scintillation of light in a turbulent biological tissue," Optik **127**, 9813–9820 (2016).
13. Y. Ata, M. C. Gökçe, and Y. Baykal, "Intensity fluctuations in biological tissues at any turbulence strength," Phys. Scripta **97**, 095501 (2022).
14. M. C. Gökçe, Y. Ata, and Y. Baykal, "Tissue turbulence and its effects on optical waves: a review," Opt. Commun. **546**, 129816 (2023).
15. A. Yariv, *Introduction to Optical Electronics* (Rinehart and Winston, 1976).
16. Y. Baykal, "Formulation of correlations for general-type beams in atmospheric turbulence," J. Opt. Soc. Am. A **23**, 889–893 (2006).
17. V. I. Tatarskii, *Wave Propagation in a Turbulent Medium* (McGraw-Hill, 1961).
18. I. S. Gradysteyn and I. M. Ryzhik, *Tables of Integrals, Series and Products* (Academic Press, 2000).
19. Y. Baykal, "Correlation and structure functions of Hermite–sinusoidal-Gaussian laser beams in a turbulent atmosphere," J. Opt. Soc. Am. A **21**, 1290–1299 (2004).
20. A. J. Radosevich, J. Yi, J. D. Rogers, *et al.*, "Structural length-scale sensitivities of reflectance measurements in continuous random media under the Born approximation," Opt. Lett. **37**, 5220–5222 (2012).
21. Q. Liang, B. Hu, Y. Zhang, *et al.*, "Coupling efficiency of a partially coherent collimating laser from turbulent biological tissue to fiber," Results Phys. **13**, 102162 (2019).
22. J. M. Schmitt and G. Kumar, "Turbulent nature of refractive-index variations in biological tissue," Opt. Lett. **21**, 1310–1312 (1996).
23. C. Andrade, "Signal-to-noise ratio, variability, and their relevance in clinical trials," J. Clin. Psychiatry **74**, 479–481 (2013).